Acta Cryst. (1988). A44, 821-827

Microstructure of U–Mo and U–W Oxides Investigated by Means of High-Resolution Electron Microscopy

BY N. D. ZAKHAROV, M. A. GRIBELYUK AND B. K. VAINSTEIN

Institute of Crystallography, Academy of Sciences of the USSR, Leninski prospekt 59, Moscow 117333, USSR

L. M. KOVBA AND S. HORIUCHI

National Institute for Researches in Inorganic Materials, Niihari-gun, Ibaraki, Japan

(*Received* 3 *December* 1987; *accepted* 8 *April* 1988)

Abstract

The potential of high-resolution electron microscopy (HREM) is demonstrated by the investigation of complex oxides with a general formula $[U_nM_mO][M_pO_{3p+1}]$, M = (Mo, W). The HREM structure images of β-UMo_2O_8 agree well with the model derived from X-ray data. It is found that the γ-$U_3Mo_{20}O_{64}$ sample considered earlier as a monophase appears in fact as a set of isostructural phases. The structure of these phases with MoO_3 octahedral block width varying within $p = 1$–7 is derived from electron microscope images. Both regular and irregular substitution of cations and the formation of uranium vacancies in M–O rows are detected in γ-$U_3Mo_{20}O_{64}$. Interstitial sites in the structures are detected, which can be occupied by extra U and W cations. The electron microscope images of vacancy rows give evidence for the finite length of some M–O rows. In this case oxygen dangling bonds at the ends of rows are supposed to be saturated by interstitial tungsten atoms.

1. Introduction

Complex oxides were the first objects in which the great possibilities of high-resolution electron microscopy (HREM) for structure investigations became apparent. On the one hand, this progress can be explained by the appearance of electron microscopes with point-to-point resolution high enough to distinguish single cations in a structure projection and to obtain unique information about structure defects and phase composition (Hashimoto, Endoh, Takai, Tomioko & Yokota, 1979; Horiuchi, 1979). The great success in HREM would not have been possible without the development of the multislice method, which was proposed by Cowley & Moodie (1957, 1959) as a tool for EM image interpretation. Practical approaches of this method to computer simulation were suggested by Goodman & Moodie (1974) and Ishizuka & Ueda (1977). The possibilities of X-ray analysis are limited in the case of complex oxides, because synthesis of sufficiently large monocrystals is still a challenging task.

We have applied the HREM method to the investigation of a number of oxides of the general formula $[U_nM_mO][M_pO_{3p+1}]$, M = (Mo, W), that are isostructural with β-UMo_2O_8. According to Mahe-Pailleret (1970) and Kovba (1971) the structure of the latter has the orthorhombic space group *Pncb* with lattice parameters $a = 7{\cdot}4$, $b = 20{\cdot}08$ and $c = 4{\cdot}115$ Å. It is built up of MoO_3 octahedral blocks extending infinitely in the **c** and **a** directions and joined by U–O rows, elongated in the **c** direction (Fig. 1). Each block is $p = 2$ octahedra thick in the **b** direction and the neighbouring octahedra are linked by corners to form an ReO_3-type structure. § 3.1 presents some results of EM investigation of β-UMo_2O_8 that agree well with this model.

It was established by means of X-ray analysis that some oxides - members of a specified series - differ from each other both in block width p and degree of partial substitution of uranium atoms by molybdenum or tungsten. The latter results in the formation of cation vacancies (Serezshkin, Kovba & Trunov, 1973, 1974). However, one should take into account that X-ray data provide the information averaged over the whole volume of the crystal. In order to obtain more detailed information (phase compositions, point defects and their ordering) two oxides, γ-$U_3Mo_{20}O_{64}$

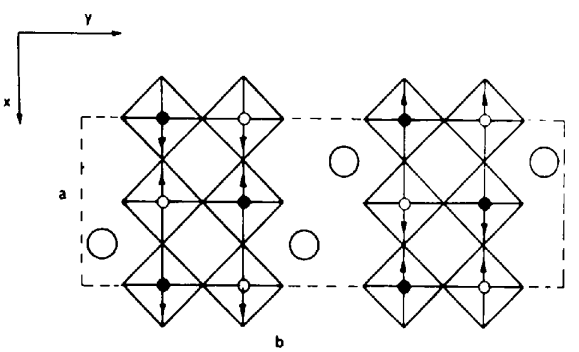

Fig. 1. Structural model of the β-UMo_2O_8 oxide in (001) projection. Open circles represent U; MoO_3 octahedra are represented schematically.

0108-7673/88/060821-07$03.00

(§ 3.2) and UW_5O_{17} (§ 3.3) were chosen for investigation. The latter oxide as well as UW_4O_{14} ($p=4$) was found earlier in a ternary oxide with bulk composition of $UMoW_{13}O_{44}$ and the structures were determined from EM images (Zakharov, Gribeluk, Vainshtein, Rozanova, Uchida & Horiuchi, 1983). Therefore we report here only on structural defects in UW_5O_{17}.

2. Experimental

The γ-$U_3Mo_{20}O_{64}$ oxide was identified as a monocrystalline phase in a sample with bulk composition $UMo_{10}O_{31}$ (Serezshkin, Ronami, Kovba & Trunov, 1974). The synthesis of $UMo_{10}O_{31}$ was carried out by annealing a weighed mixture of uranium oxide, molybdenum dioxide and molbydenum trioxide in a sealed silica tube at $T=1023$–1073 K. The $UMoW_{13}O_{44}$ oxide was synthesized in the same way at $T=1273$ K for $t=100$ h, but the mixture consisted of MoO_3, WO_3 and UO_2.

The samples were crushed in an agate mortar, dispersed in carbon tetrachloride and then collected on holey carbon film. The JEM-100B, JEM-100C and H-1250 electron microscopes, operating at accelerating voltages $U=100$ kV and $U=1$ MV were used. The objective aperture size was set to $R=0{\cdot}33$ Å^{-1} in the former cases and to $R=0{\cdot}6$ Å^{-1} in the latter. The interpretation of EM images was performed on the basis of computer simulation data using the well known Cowley multislice method. The diffraction aperture was set to $D=3$ Å^{-1}, and the slice thickness $\delta Z=2{\cdot}05$ Å. In order to account for absorption an imaginary part of the electron scattering atomic amplitude $f(g)$ was introduced in the following way: $f_i'(g)/f_i(g)=m_i$ for all g reflections. Here $f'(g)$ is the imaginary part of the atomic amplitude for the ith atom and $m_i=0{\cdot}01\ f_i(0)$.

3. Results

3.1. β-UMo_2O_8 *phase*

Our EM observations have shown that the synthesized specimen is a monophase one. A typical micrograph of this structure is presented in Fig. 2. Dark zig-zag bands correspond to the U–O rows between blocks (Fig. 1) and bright spots correspond to square channels in blocks formed by neighbouring octahedra. It should be noted that the neighbouring spots are not identical in brightness, this feature leading to periodicity $a=7{\cdot}4$ Å. As has been calculated in Fig. 3, this difference is caused by the displacement of uranium atoms from the centres of hexagonal bipyramids in the **b** direction (see Fig. 1). Less-bright spots correspond to channels to which the uranium atoms are shifted. This correlation is observed up to a crystal thickness of $t=80$ Å. The best fit of the experimental image (Fig. 2) to the calculated one was achieved at $t=60$ Å, defocus $\Delta f=-850$ Å (spherical aberation constant $C_s=1$ mm). The bright-field image in Fig. 4 presents another example, where the difference in the brightness of neighbouring spots is explained similarly to the previous case. In order to estimate the range of crystal thicknesses where the kinematical approximation can be applied to the qualitative description of the contrast, two sets of calculated images based on the multislice method and thin phase grating approximation, respectively, were simulated. Remarkable differences between corresponding 100 kV images were detected for $t>12$ Å.

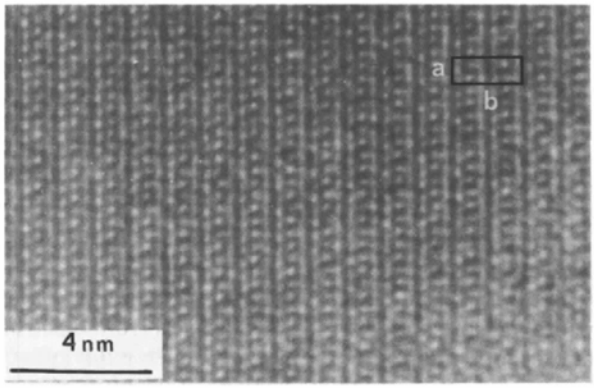

Fig. 2. 100 kV bright-field image of the β-UMo_2O_8 oxide with a unit cell shown in the upper right corner.

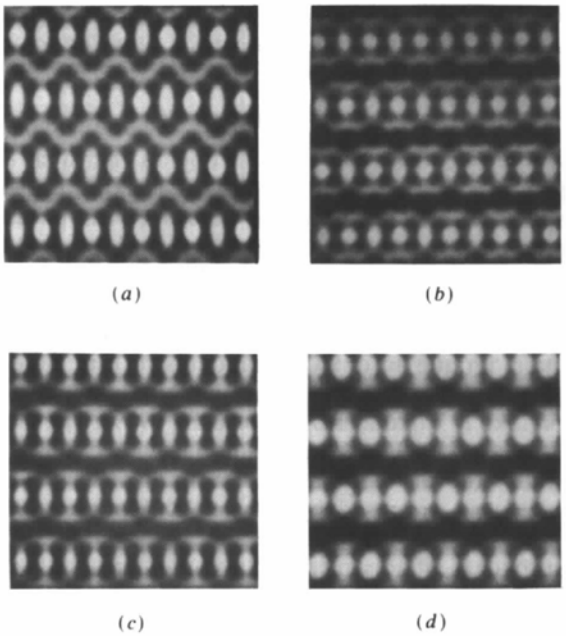

Fig. 3. A map of c-axis 100 kV calculated images of the β-UMo_2O_8 structure recorded at defocus $\Delta f=-850$ Å and crystal thickness (*a*) $t=20$, (*b*) $t=40$, (*c*) $t=60$ and (*d*) $t=120$ Å.

3.2. γ-$U_3Mo_{20}O_{64}$ *phase*

A partial substitution of uranium atoms by molybdenum in M–O rows takes place in this structure, as has been reported from X-ray data (Serezshkin, Ronami, Kovba & Trunov, 1974). At the same time vacancies are created in order to maintain charge neutrality. They have been thought to appear regularly so that the b parameter is twice as large as that of β-UMo_2O_8 oxide. The crystallochemical formula γ-$[U_{3/8}Mo_{1/2}O][Mo_2O_7]$ derived by Serezshkin, Ronami, Kovba & Trunov (1974) corresponds to the block width $p=2$.

However, our EM observations have shown that this model is only approximate. First of all it was found that the investigated samples contain several phases. This is manifested in both block width and cation occupation disorder. Bright-field images shown in Figs. 5(a) and (b) were observed in the neighbouring regions, separated by a distance of about 100 Å. The crystal thickness and imaging conditions are almost the same in both regions. However, the lattice constant a is different ($a_1=3{\cdot}7$, $a_2=7{\cdot}4$ Å), because of the difference in the substitution of uranium atoms by molybdenum in M–O rows. In the region (a) all cation positions are occupied by uranium atoms only, while in (b) an ordered alternation of U–O and Mo–O rows in the **b** direction occurs, *i.e.* –U–Mo–U–Mo–.... The chemical formulae of the two phases are UMo_6O_{20} and $UMo_{13}O_{40}$, respectively.

It should be noted that there is no sharp border between the two phases in the micrograph. Furthermore, uranium coordination polyhedra are different too: pentagonal bipyramids in the region (a) and hexagonal bipyramids in the region (b). This leads to small variation of lattice constants and, consequently, to elastic strain fields, which are detected in the image as the crystal bending contrast in the intermediate region.

Results of computer simulations correlate well with this interpretation. It should be noted that under the experimental conditions used (defocus $\Delta f=-1050$ Å, $C_s=2{\cdot}0$ mm, crystal thickness $t=70$ Å) dark vertical strips correspond in both images to MoO_3 octahedra, but in Fig. 5(b) the contrast of M–O rows is reversed: bright spots correspond to uranium atoms and dark ones to molybdenum. Some lattice distortions in blocks are visible in both images. In agreement with earlier investigations we have found that partial substitution by molybdenum is accompanied by formation of cation vacancies. Careful examination reveals that bright spots in the image

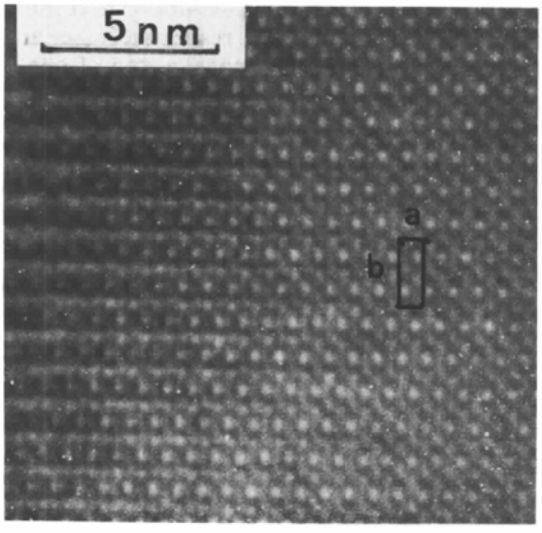

Fig. 4. 100 kV bright-field image of the β-UMo_2O_8 oxide showing the influence of shifted U atoms on the image of square channels (bright spots) in MoO_3 octahedral blocks.

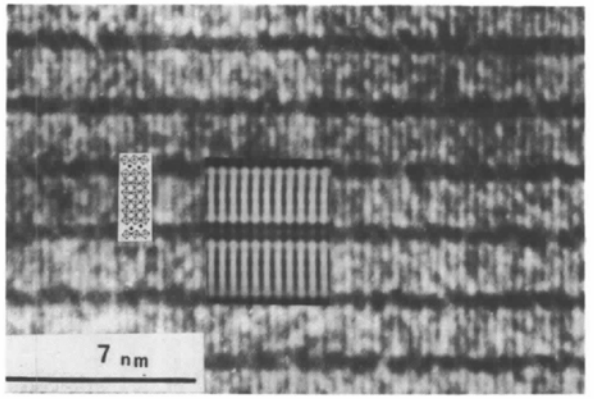

(a)

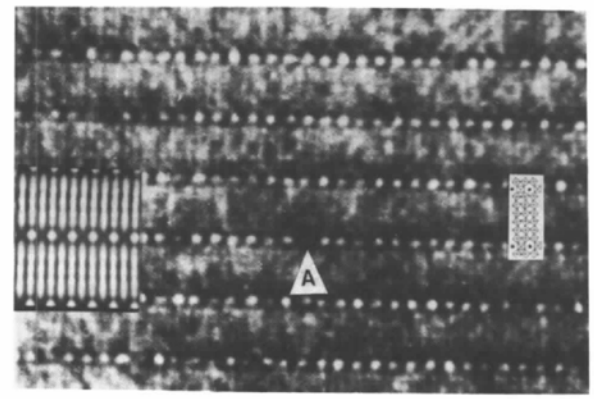

(b)

Fig. 5. 100 kV bright-field images of two neighbouring regions in a γ-$U_3Mo_{20}O_{64}$ sample; in (a) cation positions between the blocks are occupied by U atoms only, in (b) there is an alternation of U–O and Mo–O rows in sheets between the blocks. Arrow A indicates the U–O row containing cation vacancies. Structural models and calculated images are shown in the insert.

(Fig. 5*b*) differ in brightness (arrowed). As follows from calculations, the formation of vacancies in U–O rows or substitution by molybdenum leads to some darkening of bright spots and the introduction of vacancies in a neighbouring Mo–O row results in the increase of bright-spot intensity.

The disorder in the occupation of the cation positions in M–O rows is clearly visible in the image shown in Fig. 6. A good correlation with calculations is achieved at $\Delta f = -100$ to -200 Å ($C_s = 2{\cdot}0$ mm), $t = 40$ Å. Dark spots correspond here to U–O rows and bright narrow strips between them to Mo–O rows. Vacancies and the partial substitution were not taken into account in the calculations. This image is an excellent illustration of the well known fact that the electron microscope acts as a filter that supresses or peaks out some spatial frequencies on image formation. Indeed, the spatial frequency $u = 0{\cdot}27$ Å^{-1} is suppressed here and $u = 0{\cdot}135$ Å^{-1} becomes stronger. Therefore, single MoO_3 octahedra in blocks are not resolved and only M–O rows located at $r = 7{\cdot}6$ Å from each other are visible.

Dark spots in the image can be roughly divided into three groups. The first is represented by large black spots (arrow *A*). They correspond to U–O rows that contain no defects. The second is represented by smaller dark spots (arrow *E*). They correspond to rows where some uranium atoms are substituted by Mo or vacancies, but the number of vacancies is less than half of the full number of cation positions in a row. There is a majority of such spots in the image.

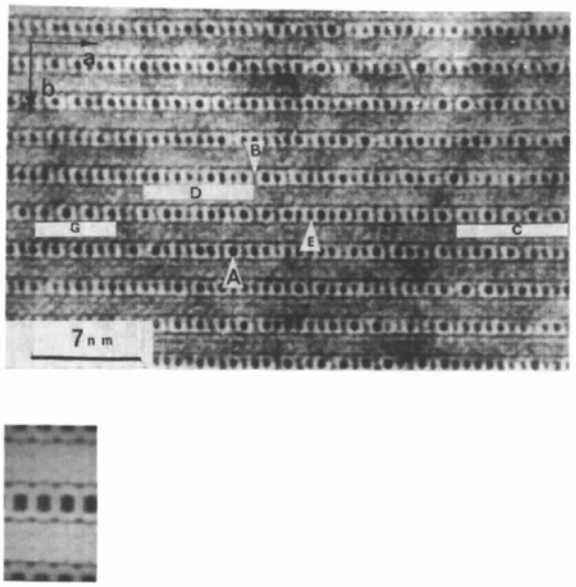

Fig. 6. 100 kV bright-field image of γ-$U_3Mo_{20}O_{64}$ in the (001) projection showing the cation disorder in M–O rows. Arrows *A*, *E* and *B* correspond to U–O rows with different numbers of cation vacancies. Parts *G*, *D* and *C* indicate different kinds of ordering of these rows. The calculated image is shown below.

The third group is represented by dim spots (arrow *B*). Their intensity is identical to that of MoO_3 octahedral blocks. If one takes into account the relation between atomic scattering amplitudes of U and Mo, this is possible only if half of the positions in a row becomes vacant (without substitution). In order to avoid dangling bonds, oxygen atoms at the row ends should form bonds with additional Mo atoms, whose octahedra share faces with octahedra in a block. Such defects were also found in UW_5O_{17} and will be discussed in more detail in the following section.

Moreover, ordering of the above-mentioned groups in the **a** direction is observed. In the combinations listed below we use the symbols 1 to 3 to indicate the corresponding group and an Mo–O row is indicated as Mo. These combinations are as follows: –2–Mo–2–Mo–... (part *D*), –2–Mo–3–Mo–2–... (part *C*) and –1–Mo–3–Mo–1–... (part *G*). However, the extension of each part is limited within 40 Å. Therefore the distribution of cations and vacancies over M–O rows should be considered as irregular on a macroscale. The existence of different kinds of ordering means that the system is far from an equilibrium state.

In addition, a number of other types of defects were found in γ-$U_3Mo_{20}O_{64}$. In contradiction to the chemical formula that corresponds to the block width $p = 2$, the phases with $p = 5$ ($UMo_{11}O_{34}$) and $p = 6$ ($UMo_{13}O_{40}$) have been most often observed. Only in rare cases were the phases with $p = 4$ and $p = 7$ detected (Fig. 7). Besides, two types of M–O rows, with cation positions occupied by uranium and molybdenum atoms respectively, form well ordered sequences in the **a** direction. Furthermore, this image demonstrates in what way phase transitions involving block width variation proceed in the system. Here the block $p = 7$ is separated by a –U–Mo– sheet into two blocks, with $p_1 = 4$ and $p_2 = 2$, respectively (see arrows *A*). As can be seen in the image, a step of one (and

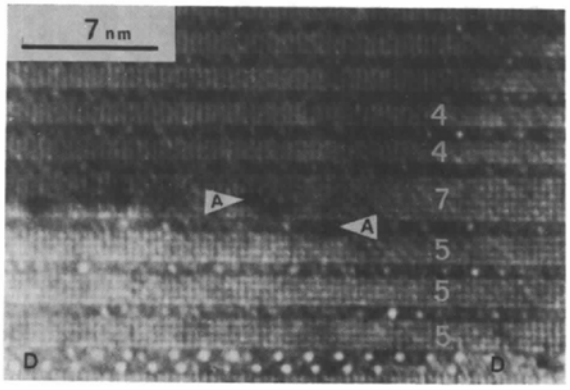

Fig. 7. 100 kV bright-field image of a γ-$U_3Mo_{20}O_{64}$ oxide showing block width disorder. Numerals indicate p values. Two *A* arrows mark the step caused by the movement of a U–O sheet. The area *D* consists of bronze-like lamellae containing U vacancies.

three) octahedra in height appears in the position of a 'jump'. The model in Fig. 8 shows that this step is formed by two neighbouring Mo atoms, which have distorted pentagonal bipyramids as coordination polyhedra.

Both single and ordered uranium vacancies were often observed in a bronze-like ($p=1$) phase (Fig. 9). Every third U–O row is absent in the ordered part, leading to structural formula $U_2Mo_9O_{30}$. The best match of calculated and experimental images is achieved at defocus $\Delta f=-700$ Å ($C_s=1$ mm) and crystal thickness $t\simeq 20$ Å.

It should be emphasized that areas with the β-UMo_2O_8 structure have also been detected in crystals under study. Bright spots in the image (Fig. 10) separated by a distance of $r=3{\cdot}7$ Å from each other correspond to channels formed by neighbouring octahedra in blocks. It is worth noting that the same correspondence was observed earlier (see Fig. 4) but the difference between neighbouring bright spots is not as large here owing to the influence of the contrast transfer function.

In summary, our data convincingly show that the γ-$U_3Mo_{20}O_{64}$ 'monophase' sample is indeed a set of phases with variable block width and different types of distribution (both statistical and ordered) of cations and associated vacancies in M–O rows.

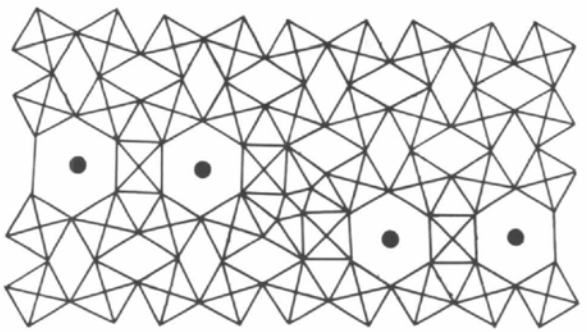

Fig. 8. Structural model corresponding to the region marked by arrows *A* in Fig. 7.

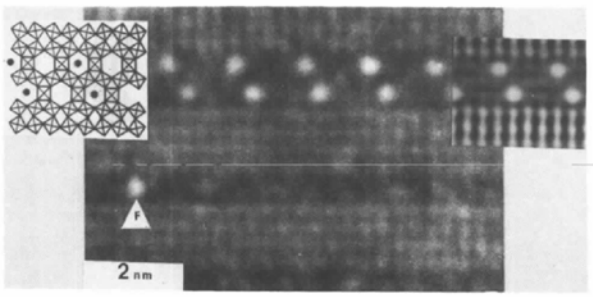

Fig. 9. Enlargement of the area *D* in Fig. 7. Cation vacancies are imaged as bright spots. Both the structural model and the calculated image are shown in the inserts.

3.3. *Structure defects in* UW_5O_{17}

We have reported a number of defects in synthesized $UMoW_{13}O_{44}$ oxides in a previous paper (Zakharov, Gribeluk, Vainshtein, Rozanova, Uchida & Horiuchi, 1983). Here the main attention is paid to the investigation of point defects in UW_5O_{17}.

Besides the variation in block width *p*, a strong disorder in the M–O rows was observed (Fig. 11). This is deduced from the variation of bright-spot intensity that corresponds to M–O rows. For example, some spots are completely absent in the

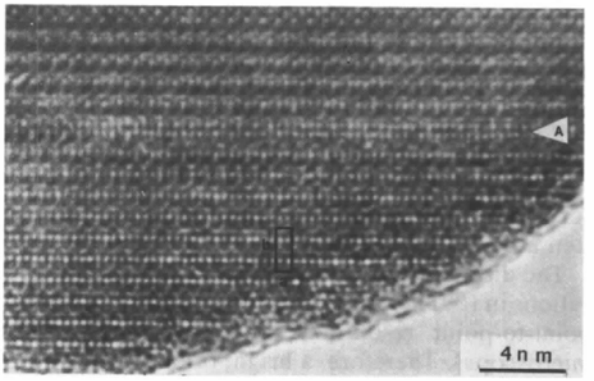

Fig. 10. 100 kV bright-field image of a β-UMo_2O_8 oxide ($p=2$) detected in a γ-$U_3Mo_{20}O_{64}$ sample. The lamella $p=1$ wide is arrowed.

(*a*)

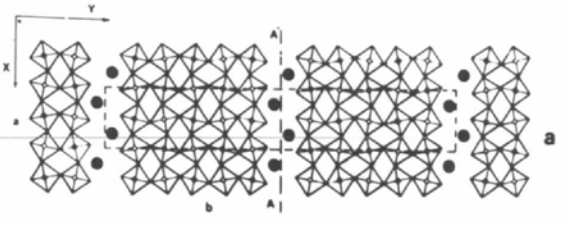

(*b*)

Fig. 11. (*a*) 1 MV *c*-axis bright-field image of a UW_5O_{17} oxide with several types of defects arrowed. (*b*) Structural model viewed along the *c* axis; filled circles represent U, MoO_3 octahedra are shown schematically.

image (arrow *A*). One can explain this by assuming a finite length of *M*–O rows. Since the distance between the ends of the rows aligning in the **c** direction is arbitrary, its value can therefore sometimes exceed the thickness of a crystal picked out for EM investigation. According to the calculations, the crystal thickness is about 50 Å. In this case all the cation positions will be vacant in some rows. Fig. 12 shows a calculated image of a line defect, where half of the cation positions are supposed to be vacant. A good agreement with the experimental image shows the validity of the proposed model.

Another interesting point concerns some bright 'bridges' between spots, which correspond to the uranium atoms in the *M*–O rows and the tungsten atoms in the MO_3 blocks (arrow *C* in Fig. 11*a*). We can assume the structure model of Fig. 13(*a*), in which an extra WO_3 octahedron shares faces with those of the original lattice. One of the oxygen atoms at the vertex of the extra octahedron belongs to a U–O row. As can be seen from the model, the interstitial tungsten atom will be observed in (001) projection.

The distance between the defect and neighbouring cations in (001) projection is shorter than $r = 2$ Å (the point-to-point resolution of the H-1250 electron microscope). Therefore, a bright bridge occurs in the image. The calculated image presented in Fig. 13(*b*) illustrates the situation with several interstitial octahedra situated along **c**. Comparison of calculated and experimental images reveals a good agreement.

It should be noted that the existence of such defects explains why the length of *M*–O rows can be finite. Indeed, no dangling bonds occur in this case because that of the last oxygen atom is 'saturated' by interstitial WO_3 octahedra. As follows from the scheme (Fig. 14*a*), the distance between the defect and neighbouring cations is about 2·6 Å, providing some evidence for direct *M*–*M* chemical bonding. For example, direct W–W bonding with cation–cation

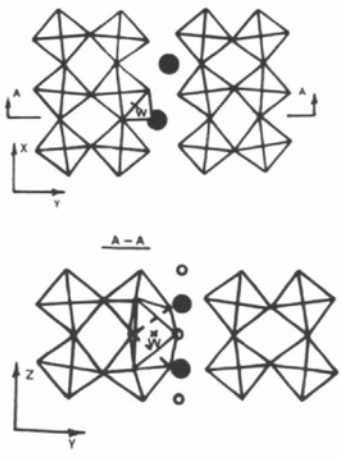

(*a*)

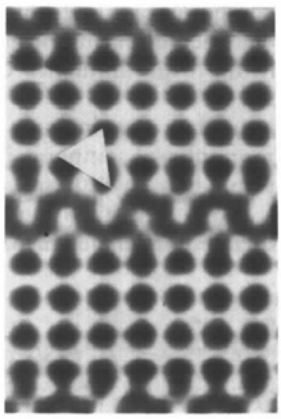

(*b*)

Fig. 13. (*a*) The model showing thee position of the extra WO_3 octahedron in (001) and (010) projections; ● U, ○ O. (*b*) The corresponding simulated image with several extra WO_3 octahedra in a row (compare with arrow *C* of Fig. 11*a*).

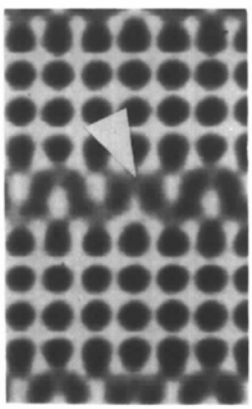

Fig. 12. The calculated image of a linear defect (arrowed) consisting of a number of cation vacancies in a U–O row (defocus $\Delta f = -900$ Å).

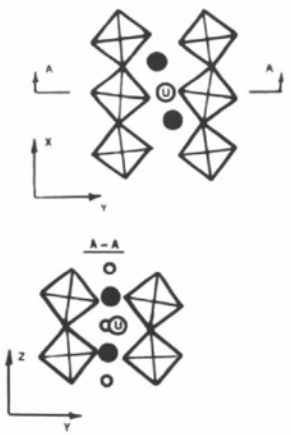

Fig. 14. Structure model showing the position of an extra U atom both in (001) and (010) projections.

distances $r = 2{\cdot}791$ and $r = 2{\cdot}53$ Å was found by Bino, Cotton, Dori & Sekutowski (1978).

One more typical image is marked by the arrow *B* in Fig. 11(*a*): a bright 'bridge' is observed here between the spots that correspond to the U–O rows. The pentagonal bipyramid is a coordination polyhedron of an extra uranium atom (Fig. 14) that shares faces with four neighbouring pentagonal bipyramids of the original lattice. Computer simulation results (Fig. 15) allow one to estimate the number of extra uranium atoms in a 'defect' column. For the arrowed image the respective occupancy ratio amounts to 50–70% of the full number of cation positions in the ideal *M*–O row. Unfortunately, we could not determine if there is any bonding between neighbouring point defects in the 'defect' column or whether their distribution is a statistical one.

The existence of these point defects leads to an excess of cations, *i.e.* the ratio of concentrations

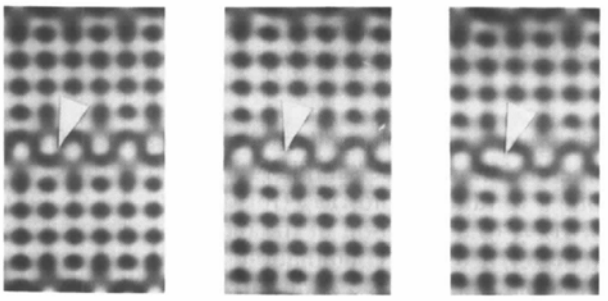

(*a*) (*b*) (*c*)

Fig. 15. A map of calculated images of a defect, formed by different numbers *N* of extra uranium atoms. The *N* value amounts to (*a*) 50%, (*b*) 70%, (*c*) 100% of the total number of cation positions in the U–O row.

C_O/C_W, C_O/C_U decreases. Thus, HREM investigations make it possible to establish what kind of stoichiometric errors might take place during the process of crystal growth.

The authors are very indebted to Dr O. A. Kolchin and Dr E. V. Orlova from the Institute of Crystallography, Moscow for the provision of the program package for the output of simulated images in the grey-level display. We are also grateful to Dr O. N. Rozanova from the Moscow State University for helping with crystal synthesis.

References

Bino, A., Cotton, F. A., Dori, Z. & Sekutowski, J. C. (1978). *Inorg. Chem.* **17**, 2946–2950.

Cowley, J. M. & Moodie, A. F. (1957). *Acta Cryst.* **10**, 609–619.

Cowley, J. M. & Moodie, A. F. (1959). *Acta Cryst.* **12**, 360–366.

Goodman, P. & Moodie, A. F. (1974). *Acta Cryst.* A**30**, 280–290.

Hashimoto, H., Endoh, H., Takai, Y., Tomioko, H. & Yokota, Y. (1979). *Direct Imaging of Atoms in Crystals and Molecules.* Proc. of the 47th Nobel Symp., edited by L. Kihlborg, pp. 23–31. Stockholm: Royal Swedish Academy of Sciences.

Horiuchi, S. (1979). *Direct Imaging of Atoms in Crystals and Molecules.* Proc. of the 47th Nobel Symp., edited by L. Kihlborg, pp. 75–81. Stockholm: Royal Swedish Academy of Sciences.

Ishizuka, K. & Ueda, N. (1977). *Acta Cryst.* A**33**, 740–749.

Kovba, L. M. (1971). *Radiochimija*, **13**, 909–910.

Mahe-Pailleret, P. (1970). *Rev. Chim. Minér.* **7**, 807–848.

Serezshkin, V. N., Kovba, L. M. & Trunov, V. K. (1973). *Kristallografiya*, **18**, 961–965.

Serezshkin, V. N., Kovba, L. M. & Trunov, V. K. (1974). *Kristallografiya*, **19**, 379–382.

Serezshkin, V. N., Ronami, G. N., Kovba, L. M. & Trunov, V. K. (1974). *Zh. Neorg. Khim.* **19**, 1036–1039.

Zakharov, N. D., Gribeluk, M. A., Vainshtein, B. K., Rozanova, O. N., Uchida, K. & Horiuchi, S. (1983). *Acta Cryst.* B**39**, 575–579.